11th International Symposium on Turbulence and Shear Flow Phenomena (TSFP11)
Southampton, UK, July 30 to August 2, 2019

DISPERSION OVER MULTISCALE ROUGH PATCHES

Claudia Nicolai
Faculty of Engineering and Physical Sciences
University of Southampton
Southampton, UK
C.Nicolai@soton.ac.uk

Mantas Gudaitis
Faculty of Engineering and Physical Sciences
University of Southampton
Southampton, UK
M.Gudaitis@soton.ac.uk

Christina Vanderwel
Faculty of Engineering and Physical Sciences
University of Southampton
Southampton, UK
C.M.Vanderwel@soton.ac.uk

ABSTRACT

In this work, we experimentally investigate the effect of a multiscale patch of roughness on the dispersion of a passive scalar near the ground. Passive fluorescent dye is released from a ground level point source upstream of the patch in a boundary layer that is naturally developing in a water tunnel. Planar laser-induced fluorescence (PLIF) and particle image velocimetry (PIV) are used to carry out measurements of concentration and velocity in the domain downstream of the point source. The spread of the mean concentration distributions for several different patches are compared with the smooth wall case to investigate the effect of patch solidity. These effects are then related to measurements of the internal boundary layer of the patch's wake.

INTRODUCTION

The problem of accurately predicting the dispersion of gas released from a point source in a turbulent boundary layer has been growing in importance, mainly due to ever-increasing urbanization rates and environmental concerns. Previous research on this topic has explored in depth the development of concentration plumes in neutral turbulent boundary layers over smooth surfaces, highlighted by the wind tunnel tests using hotwires, flame-ionisation detectors, and photo-ionisation detectors by Fackrell & Robins (1982), Mavroidis & Griffiths (2001) and Talluru et al. (2017).

The effects of surface obstacles on dispersion have previously been studied for a limited range of surface conditions: Vinçont et al. (2000) previously investigated the effect a single cubic obstacle has on dispersion and Macdonald et al. (1998) studied field tests of dispersion through a regular array of cubes. In the present work, we extend this research to investigate dispersion around a finite patch of multiscale roughness, typical of an isolated urban development.

For such abrupt changes in the surface conditions, an internal boundary layer is expected to develop at the roughness transition denoting the extent that the new surface conditions affect outer similarity (Mahrt, 2000). In this work, we aim to investigate how this internal boundary layer influences mixing.

EXPERIMENTAL METHODS

Experimental technique and setup

In order to assess the dispersion characteristics in the wake of multiscale rough patches interacting with a turbulent boundary layer, particle image velocimetry (PIV) and planar laser induced florescence (PLIF) techniques have been applied simultaneously in the test section of a closed loop water tunnel, with a width of 1200 mm and a length of 6250 mm. During the measurements, the water depth was kept constant to 600 mm and the free stream velocity set at $U_\infty \approx 0.45$ m/s. The rough patch was mounted flush with the floor of the tunnel, 5550 mm downstream of the test section entrance, embedded in a false floor of clear acrylic that spanned the entire test section extent. A thin tube (3 mm inner diameter) was embedded in the false floor and supplied Rhodamine 6G dye at a rate of 30 cc/min so as to create a point source at the wall located 5 mm upstream of the patch, having minimal disturbance to the flow.

The investigation domain consists of a vertical-streamwise plane, located in the centre of the water tunnel and extending over two patch diameters. This was achieved by combining two successive experiments in two contiguous sections (see schematic in Figure 1): the first one including the patch and the source upstream, the second one immediately downstream, partially overlapping the first one. In each section, the field of view was illuminated by a Nd:YAG 100mJ pulsed laser operating at 4Hz. A pair of 4 MP CMOS cameras were used for the PIV measurements, equipped wavelength filters to filter out the PLIF signal.

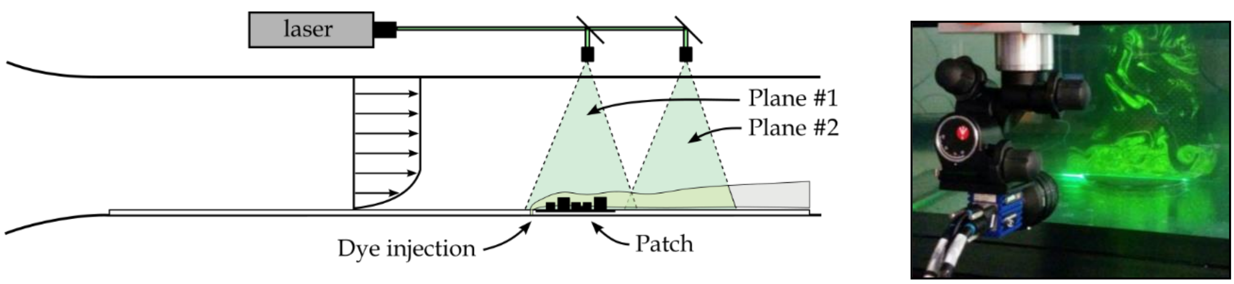

Figure 1. (Left) Schematic of the experimental arrangement, illustrating PIV-PLIF measurements in two fields of view in the streamwise wall-normal plane. (Right) Photograph of one of the cameras and the fluorescent dye illuminated by the laser.

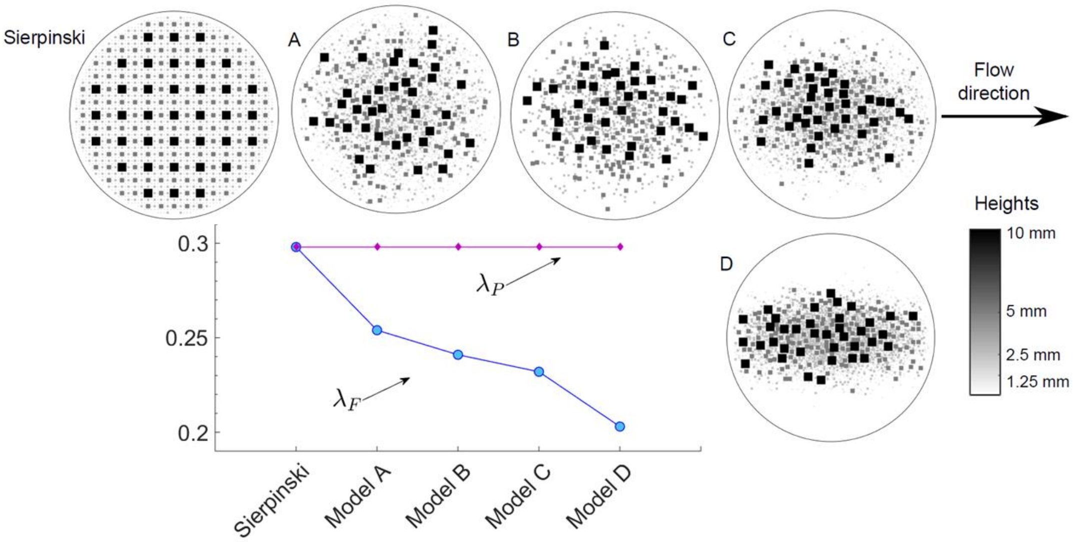

Figure 2. Rough patches. Sierpinski with cubes regular arrangement, $\lambda_F = 0.298$. A, random arrangement, $\lambda_F = 0.254$. B, random, $\lambda_F = 0.241$. Model C, random, $\lambda_F = 0.232$. D, random, $\lambda_F = 0.203$.

A third 5.5 MP 16-bit sCMOS camera simultaneously captured the PLIF measurements, equipped with a wavelength filter to block all light except the PLIF signal (Vanderwel & Tavoularis, 2014). An inline power energy monitor measured the laser power of each pulse so as to reduce the uncertainty of the concentration measurements. To maximise the signal to noise ratio of the concentration measurements, the concentration of the dye solution at the source (C_S) was set to 0.3 mg/L at the first section, while in the second section $C_S = 10$ mg/L, and all concentration measurements are normalised by C_S during processing.

Design of the rough patches

Rough patches (displayed in figure 2) were designed and 3D-printed in polyamide using regular and random arrangements of four scales of cubes (10 mm, 5 mm, 2.5 mm, and 1.25 mm) distributed within a diameter of 240 mm. The different arrangements vary the frontal solidity, λ_F, of the patches while maintaining the planform solidity, λ_P, and height distributions constant. The frontal solidity λ_F is defined as the ratio between the total forward-facing surface and the platform surface, hence indicative of the blockage experienced by the incoming flow. The regularly organized pattern is inspired by the three-dimensional counterpart of the Sierpinski carpet and has a frontal solidity of 0.298. By randomizing this pattern, four different models have been generated with a decreasing frontal solidity: between 0.254 and 0.203 from model A to D as displayed by the chart in figure 2. The properties of the wake developed past the same configurations have been the subject of a previous investigation as described by Vanderwel & Ganapathisubramani (2018).

RESULTS

Smooth wall measurements

The dispersion of a ground level point source over a smooth wall was measured in order to validate our measurements against previous work and to provide a baseline for the effects of the rough patches. The boundary layer thickness of the smooth-wall boundary layer is $\delta \approx 80$ mm. The friction velocity u_τ was evaluated from the near-wall peak of the Reynolds shear stress, resulting in $u_\tau = 0.018$ m/s ± 5%. With this, the dimensionless velocity is plotted in Figure 3 and the law of the wall is fit to the logarithmic region following

$$U^+ = \frac{U}{u_\tau} = \frac{1}{\kappa}\ln\left(\frac{y}{\delta_\nu}\right), \qquad (1)$$

where the von Karman constant $\kappa = 0.38$. The viscous lengthscale was consistently $\delta_\nu = 0.2$ mm ± 15%.

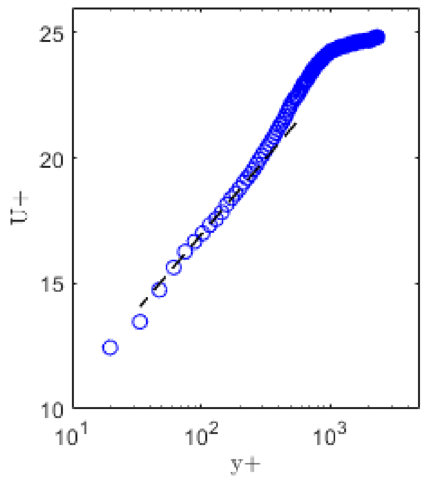

Figure 3. Log-law fit to the baseline turbulent boundary layer flow over the smooth wall.

The mean concentration and concentration variance maps over the smooth surface are reported in figure 4. We verified that the magnitudes of the measurements from the two fields of view were consistent by checking a cross-section of the concentration at y = 5mm, which followed a continuous exponential decay function away from the source as expected.

Concentration profiles along the wall-normal direction, extracted at several fixed streamwise locations (x/ δ = 2.5-4.5), are presented in figure 5.

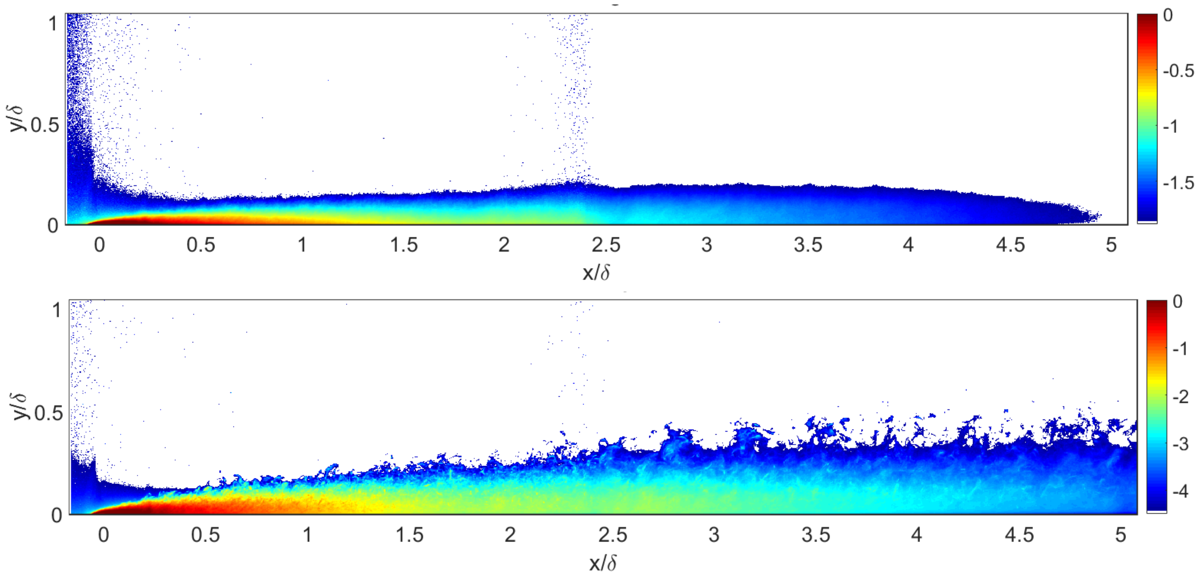

Figure 4. (Top) Mean logarithmic concentration map, $\log_{10}(C/C_S)$, over smooth wall boundary layer. (Bottom) Map of concentration variance ($\log_{10}(c^2/C_S{}^2)$).

As in Fackrell and Robins (1982), the scalar concentration peaks at the wall and decays in the streamwise direction preserving the shape such that the mean concentration profiles can be modelled by the well-established empirical relation proposed by Robins (1978):

$$C = C_0 \exp(-\ln(2)(y/\sigma_y)^2), \quad (2)$$

where C_0 is the peak concentration at the wall and σ_y is the plume halfwidth, determined from the second moment of the concentration distribution (displayed in figure 6). Figure 7 (left) displays the remarkable collapse of the scaled data; the empirical law is also reported for comparison. The streamwise growth of the plume halfwidth is indicative of the plume spread, and according to the previous literature the growth is described by a power law; in figure 6, the halfwidth is reported along with the best fit confirming the power law behaviour, namely the plume halfwidth decays as $\sigma_y \sim x^{0.73}$. The variance, displayed in figure 7 (right), exhibits the expected self-similarity once the profiles are normalized with the plume halfwidth and the peak value of the variance, $c_0{}^2$. The location of $c_0{}^2$ roughly coincides with $y/\sigma_y \approx 0.5$, hence away from the wall consistently with the location of maximum production.

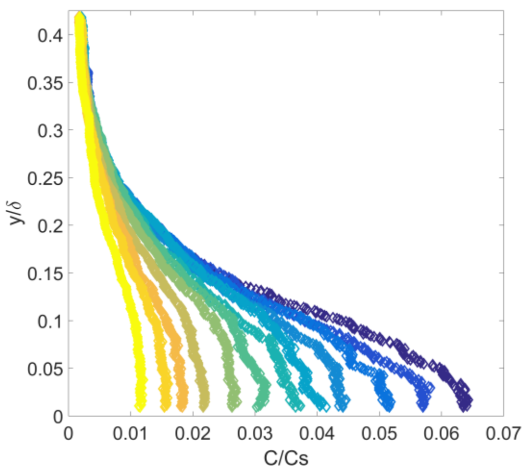

Figure 5. Mean concentration profiles at (x/ δ = 2.5-4.5).

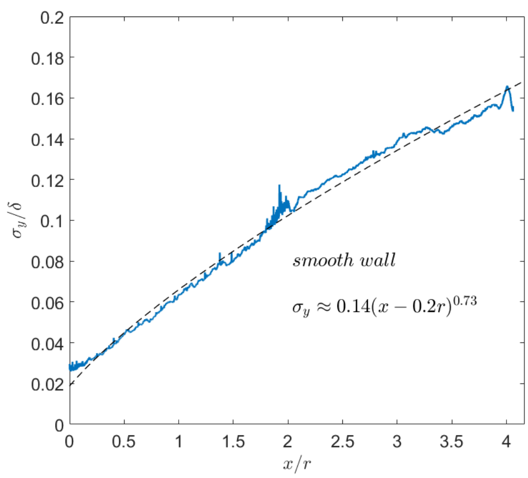

Figure 6. Plume halfwidths over the smooth wall.

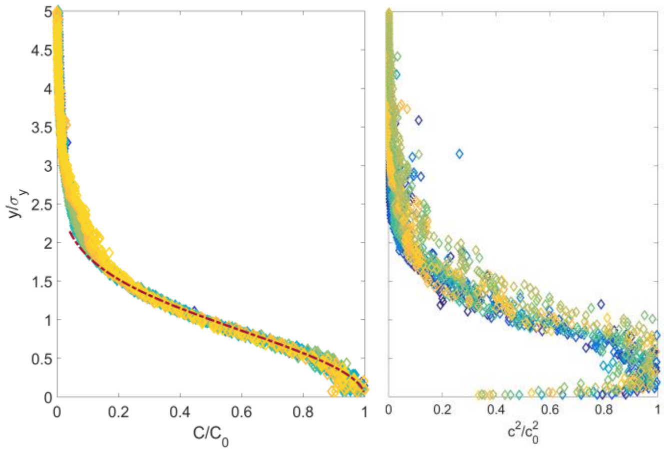

Figure 7. (Left) Scaled mean concentration (symbols) and empirical law (red dashed line). (Right) Scaled concentration variance.

ROUGH PATCHES RESULTS

Internal boundary layer

The internal boundary layer resulting from each patch was determined from the PIV measurements by mapping the velocity deficit as

$$\Delta\overline{U} = \overline{U}_{ref} - \overline{U}, \qquad (3)$$

where $\overline{U}_{ref}$ is the mean streamwise velocity field measured over the smooth wall. This is presented in Figure 9 for the patch with cubes regularly arranged and indicates that the internal boundary layer remains within the lower part of the boundary layer, $y/\delta < 0.40$. The extent of the internal boundary layer δ_I is defined as the contour $\Delta\overline{U}/U = 5\%$ and is plotted in Figure 8 for all the patches.

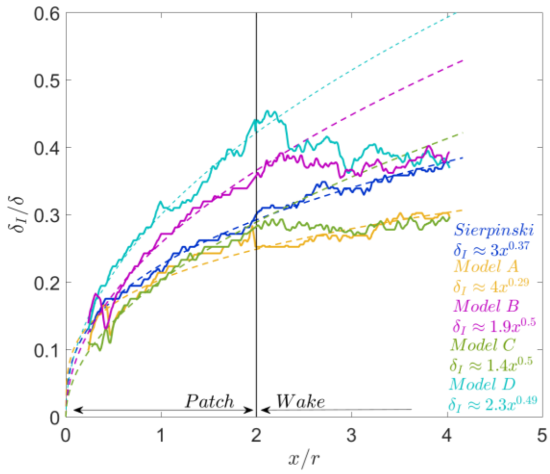

Figure 8. Internal boundary layer over rough patches.

characterized by a lower frontal solidity, display a larger δ_I. In the wake ($x > 2r$), the global trend is still non-monotonic, but a substantial difference is detected between the organized arrangement (Sierpinski) and the random models: while the former presents a growing δ_I, the latter ones present a decaying δ_I. The lack of a monotonic behaviour can be explained considering that both flow and concentration behaviour on the central plane is only partially representative of the global behaviour due to 3D effects triggered by the cubes spatial arrangement, while frontal solidity and drag are global indicators. Furthermore, a fitting procedure has been carried out to detect the growth of the internal boundary layers, the fitting curves are displayed in figure 8. Globally, δ_I exhibits a power law behaviour over the patches regardless the specific morphology. While a power law growth rate is globally established, the value for the exponent varies in the range 0.22-0.86 consistent with Rouhi at al. (2019). For the present investigation, the morphology seems to play a role in setting the exponent: for the organized pattern δ_I scales as $x^{0.37}$; for models B-C $\delta_I \sim x^{0.5}$; while the model A represents an exception behaving closer to the organized model than to the random ones, namely $\delta_I \sim x^{0.29}$.

In the wake region, past the patches, the internal boundary layer of the model "Sierpinski" keeps following the power law behaviour found over the patch, as model A does; while for models B-C a clear departure from the power law is detected, i.e. δ_I is found to progressively deviate from the power law at increasing frontal solidity. A decaying trend arises for model C.

Plume halfwidth

The mean concentration map corresponding to the regular arrangement patch is presented in Figure 10. High concentration zones seem to remain confined among and as for the random organized ones (not shown here). These results are consistent with the findings of Macdonald et al. (1998), who observed that the mean concentration field over an array of cubes was 2–3 times larger than that in open terrain, and exhibited a large initial deflection in the near field due to the

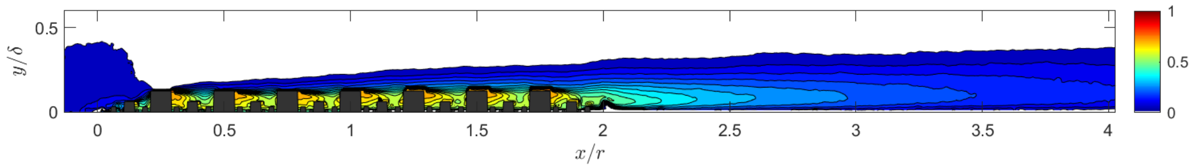

Figure 9. The velocity deficit $\Delta\overline{U} = \overline{U}_{ref} - \overline{U}$ contour map over the patch with the regular arrangement.

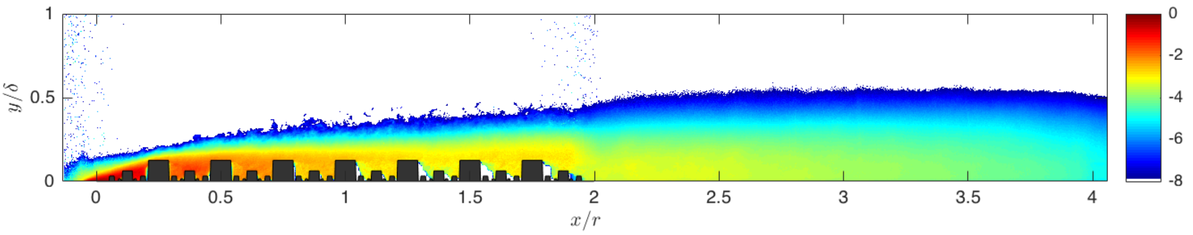

Figure 10. The mean concentration $\log_{10}(C/C_S)$ map over the patch with the regular arrangement.

The thickness of the internal boundary layer is supposed to depend on frontal solidity: a progressively lower frontal solidity should correspond with a progressively thinner δ_I, according to the drag behaviour reported in Vanderwel & Ganapathisubramani (2019); while, in figure 8, the behaviour of δ_I is not monotonic with respect to λ_F. In particular, over the patches ($x < 2r$), the Sierpinski model and models A and C present very similar results for δ_I, while models B and D,

obstacles. Although $\delta_I > \sigma_y$, note that some dye does appear to penetrate the edge of internal boundary layer, which is apparent when comparing Figures 9 and 10.

In open terrain, namely in the near wake of the patch, the growth trend of the internal boundary layer can be compared to the growth of the plume halfwidth. We only present the plume halfwidth in the wake region as the presence of the cubes greatly biases this measurement over the patch. These results are displayed in figure 11 a-e. For the regular patch and the randomly organized ones with lower frontal solidity, σ_y appears to follow the growing trend of the internal boundary layer; while for models B-D, a growing plume halfwidth combines with a progressively decaying δ_I. Furthermore, over these models the plume seems to penetrate further up.

DISCUSSION

In order to detect any correlation between the internal boundary layer and the plume growth, we define an alternative measure for the plume edge: we detect the edge, θ, as a contour line on which the concentration value is 0.005 times the source concentration. This is an arbitrary value, allowing for the edge to be not biased by the local morphology of the patch. The contour lines pertaining the assessed models are displayed in figures 11 a-e, together with δ_I. We need to point out that the possibility to detect a given contour line is affected by the dilution due to the turbulent mixing, this means that a given concentration exists only for a certain extent, for this reason we consider the plume edge until x = 3r for fitting purposes, where $C = 0.005C_S$ is detectable for the all patches.

For the organized patch (figure 11 a) the plume edge seems to follow the growth trend of the internal boundary layer. θ scales as $x^{0.3}$, both over the patch and in the near wake, this is similar to the scaling detected for the internal boundary layer, namely $\delta_I \sim x^{0.37}$. For the random patches B-C (figures 11 c-d), θ seems to follows the internal boundary layer just over the first half of the patch, where, in fact, θ scales as x^α with α = (0.5-0.55). Hence the plume edge is proportional to the internal boundary layer. Model A (figure 11 b) is again an *unicum*: a power law seems to capture θ only in a small portion over the patch, namely for 0.5 < x < 1.5, where the plume edge scales as $x^{0.3}$.

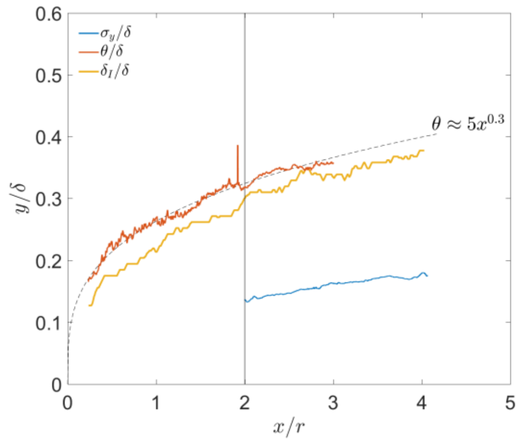

a)

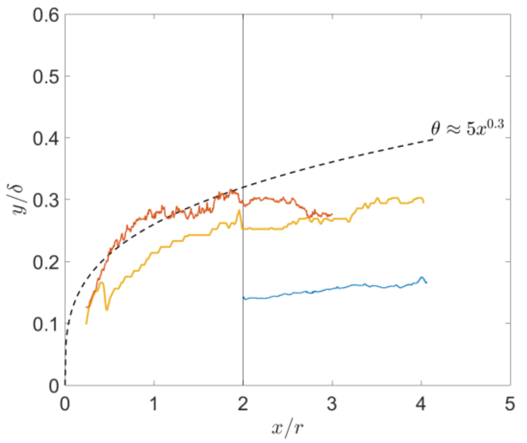

b)

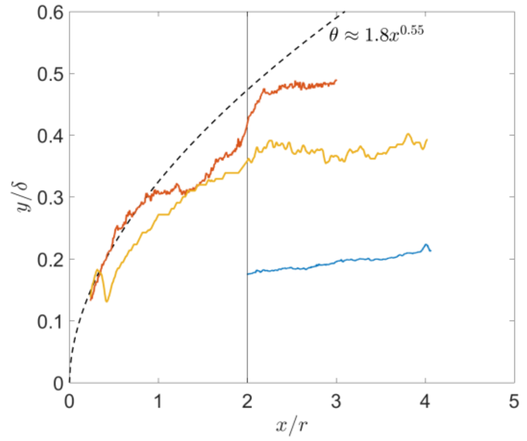

c)

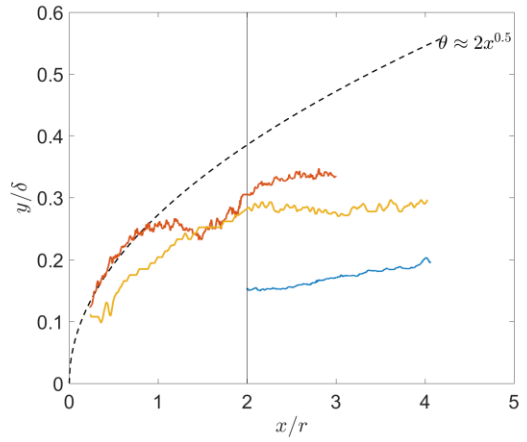

d)

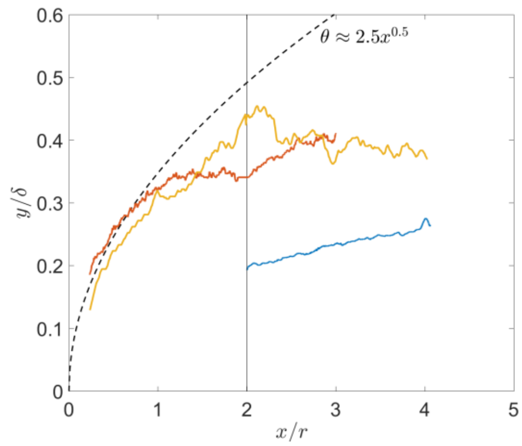

e)

Figure 11. a-e) Sierpinski and Models A-D, respectively. Red line: Concentration contour line (θ). Yellow line: internal boundary layer thickness (δ_I). Blue line: plume halfwidth (σ_y).

CONCLUSION

In this experimental study, the dispersion of a scalar, released from a wall point source, interacting with patches of roughness, has been addressed applying PIV and PLIF simultaneously. The inspection of mean concentration maps reveals that, in the presence of rough patches, high concentration zones can be identified among the roughness elements. The interaction between the incoming flow and the patches has been quantified, in terms of the velocity field, by the thickness of the internal boundary layer (δ_I) growing over the patch: its behaviour over the patches is well captured by a power law, with an exponent that seems to depend on the surface morphology. The same power law only partially captures the trend of the plume edge, when detected as a contour line of the mean concentration field. In the patches' near wake, the plume halfwidth (σ_y) has been compared to the internal boundary layer, revealing that: while σ_y grows spreading away from the wall, consistently with the increasing frontal solidity, δ_I shows an incipient decay. Further investigation is needed to clarify the role of the internal boundary layer in modulating the scalar dispersion. The analysis presented in this paper will be extended to higher order statistical moments of velocity and concentration fields to provide motivation for the growth trend identified for the plume edge and the internal boundary layer.

REFERENCES

Fackrell, J. and Robins, A. (1982). Concentration fluctuations and fluxes in plumes from point sources in a turbulent boundary layer. Journal of Fluid Mechanics, 117, 1-26.

Macdonald, R., Griffiths, R. and Hall, D. (1998). A comparison of results from scaled field and wind tunnel modelling of dispersion in arrays of obstacles. Atmospheric Environment, 32(22), 3845-3862.

Mahrt, L. (2000). Surface heterogeneity and vertical structure of the boundary layer. Boundary-Layer Meteorology 96(1), 33–62.

Mavroidis, I. and Griffiths, R.F. (2001). Local characteristics of atmospheric dispersion within building arrays. Atmospheric Environment, 35(16), 2941-2954.

Rouhi, A., Chung, D., and Hutchins, N.. "Direct numerical simulation of open-channel flow over smooth-to-rough and rough-to-smooth step changes." Journal of Fluid Mechanics 866 (2019): 450-486.

Talluru, K., Hernandez-Silva, C., Philip, J. and Chauhan, K. (2017). Measurements of scalar released from point sources in a turbulent boundary layer. Measurement Science and Technology, 28(5), 055801.

Vanderwel, C., and Tavoularis, S. (2014). On the accuracy of PLIF measurements in slender plumes. Experiments in Fluids, 55:1801.

Vanderwel, C., and Ganapathisubramani, B. (2019). Turbulent boundary layers over multiscale rough patches. Boundary Layer Meteorology.

Vinçont, J., Simoëns, S., Ayrault, M. and Wallace, J. (2000). Passive scalar dispersion in a turbulent boundary layer from a line source at the wall and downstream of an obstacle. Journal of Fluid Mechanics, 424, 127-167.